SCIENCE CHINA
Technological Sciences

•Article•

December 2018 Vol.61 No.12: 1866–1871
https://doi.org/10.1007/s11431-017-9200-6

Measurements of convection electric field in the inner magnetosphere

LV Xin & LIU WenLong*

School of Space and Environment, Beihang University, Beijing 100191, China

Received September 11, 2017; accepted January 18, 2018; published online October 19, 2018

In this paper, we study the characteristic of large-scale convection electric field in the inner magnetosphere, using magnetospheric multiscale (MMS) observations between L=5 and L=8 over the period from September 1, 2015 to October 31, 2016, covering almost all magnetic local time (MLT). Observations show that the DC convection electric field generally has small variations in this region. We investigate whether the convection electric field is correlated with geomagnetic indices and solar wind parameters. It is found that, among the studied parameters, solar wind electric field, z component of interplanetary magnetic field, AE and Kp indices show good correlations with the averaged convection electric field. The results in this paper provide valuable information for understanding the role of electric field on the dynamics of the inner magnetosphere.

convection, electric field, inner magnetosphere

Citation: Lv X, Liu W L. Measurements of convection electric field in the inner magnetosphere. Sci China Tech Sci, 2018, 61: 1866–1871, https://doi.org/10.1007/s11431-017-9200-6

1 Introduction

The large-scale convection electric field plays an important role in the dynamics and structures of the inner magnetosphere, such as the plasmasphere, ring current, the outer radiation belt and plasma sheet [1–7]. It is well known that dawn-dusk quasi-static electric field can be produced by the interaction of the solar wind flowing past the Earth's magnetic field with the magnetosphere, driving sunward plasma convection from the magnetotail [8–13]. This sunward convection transports plasmas to the inner magnetosphere and therefore the plasmas are dominated by the **E**×**B** or gradient **B** drift motion, depending on the energy of plasmas [14–19]. Curvature and gradient drifts cause electrons to drift eastward and ions to drift westward leading to the formation of the ring current. The electric field is, in turn, affected by the ring current particles through magnetosphere-ionosphere (M-I) coupling [20,21]. It is therefore crucial to have accurate information of the electric field in order to understand the dynamics of the inner magnetosphere.

Volland [22] and Stern [23] developed a semi-empirical model, known as Volland-Stern model, of the electric field in the inner magnetosphere. The Volland-Stern model predicts that, in the corotating frame of the Earth, the electric field should diminish in intensity closer to Earth due to shielding effects. Rowland and Wygant [24] studied the large-scale dawn-dusk electric field in the inner magnetosphere using data from the Combined Release and Radiation Effects Satellite (CRRES) mission, and found that the electric field is in relation to the Kp geomagnetic index. It is revealed that the electric field is related to the Kp and L shell and has a local maximum in the electric field developing near Earth during active times, rather than the expected enhancement at higher L shells as suggested by the Volland-Stern model. During active times, electric field was found to enhance as low as L<3 [24]. Califf et al. [8] verified this work with Time

* Corresponding author (email: liuwenlong@buaa.edu.cn)

History of Events and Macroscale Interactions during Substorms (THEMIS) mission observations, which provided more complete local time coverage. That study offered a picture of the dawn-dusk electric field covering all local times and radial distances in the inner magnetosphere, and the results reached agreement with the CRRES observations in the duskside.

Baumjohann et al. [25,26] studied electric field at the geosynchronous orbit using data from the Geodetic Earth-Orbiting Satellite 2 probe (GEOS 2) electron gun experiment. They investigated the dependence of the convection electric field on solar wind and interplanetary magnetic field (IMF) conditions, and found *Kp*, IMF_B_z and IMF_B_y dependences as well as the local time dependence of the electric fields at L=6.6.

In this paper, we will investigate the characteristic of large-scale electric field based on the new electric field measurement from the MMS mission. The dependence of the electric field on the geomagnetic activity and the solar wind condition will be examined to improve our understanding of the electric field in the inner magnetosphere.

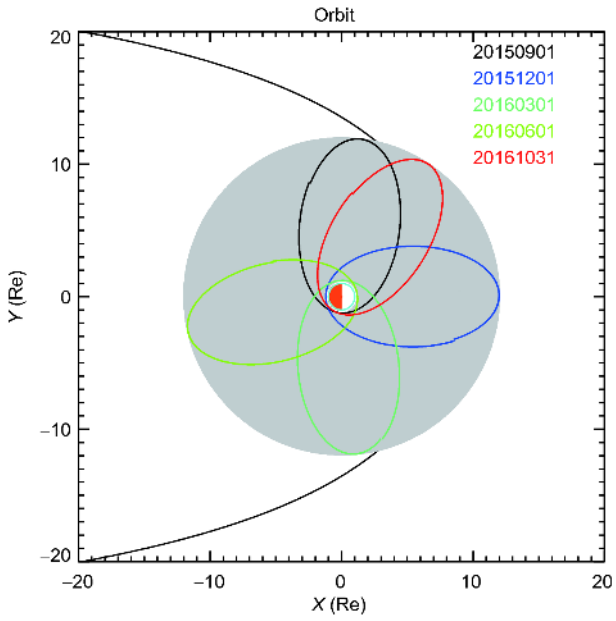

Figure 1 (Color online) The orbits of MMS-1 satellite on September 1, 2015, December 1, 2015, March 1, 2016, June 1, 2016 and October 31, 2016. The magnetopause location is calculated by Shue et al. [28] model for SW_Dp=5 nPa and IMF_B_z=0 nT.

2 Instrumentation

The four identical MMS probes were launched on March 12, 2015 with apogee at 12 Re and perigee at about 1.5 Re in a tetrahedron formation with separations of ~15 km [27]. Because of their small spatial separation, the convection electric fields observed by the four probes are similar. Therefore, we only use data from MMS-1 probe in this study. From September 2015 to October 2016, MMS spacecraft completes a full coverage of local time, as shown in Figure 1 [28].

Each spacecraft is equipped with FIELDS suite that provides electric field and magnetic field measurements in three dimensions [29]. The magnetic field, electric field and spacecraft potential data used in this study are provided by the Electric Field Double Probe (EDP) and the Fluxgate Magnetometer (FGM).

The Axial Double Probe (ADP) and the Spin Plane Double Probes (SDP) are the two components of EDP, measuring 3D electric field [30,31]. The ADP instrument measures the DC to ~100 kHz electric field along the spin axis of the MMS spacecraft [30]. The SDP measures the electric field in the spin plane with an accuracy of 0.5 mV/m over the frequency range from DC to 100 kHz. SDP consists of 4 biased spherical probes extended on 60 m long wire booms 90° apart in the spin plane, giving a 120-m baseline for each of the two spin-plane electric field components [31]. In the current study, only the measurements of the y component of electric field in GSE (Geocentric Solar Ecliptic) coordinate are used.

Solar wind parameters and geomagnetic activity indices are obtained from the Coordinated Data Analysis Web (https://cdaweb.gsfc.nasa.gov/sp_phys).

3 Data processing

This study uses valid electric field measurements from MMS-1 probe between September 1, 2015 and October 31, 2016. The electric field data are provided in slow survey (SS) mode, fast survey (FS) mode and burst mode. In the inner magnetosphere, the electric field data are mostly in SS mode with time resolution of 0.125 s.

In order to calculate the convection electric field in the co-rotating frame, we convert the measured electric field in the spacecraft frame to inertial frame, and then subtract the co-rotation electric field. Thus, large-scale convection electric field in the co-rotating frame can be given as

$$\mathbf{E}_{\text{convection}} = \mathbf{E}_{\text{obs}} - \mathbf{V}_{\text{sc}} \times \mathbf{B} + \boldsymbol{\omega} \times \mathbf{R} \times \mathbf{B}, \quad (1)$$

where $\mathbf{E}_{\text{obs}}$ is the electric field in the spacecraft frame measured by MMS EDP instrument, $\mathbf{V}_{\text{sc}}$ is the spacecraft velocity vector, $\mathbf{B}$ is the measured magnetic field, $\boldsymbol{\omega}$ is the Earth's angular velocity vector, $\mathbf{R}$ is the spacecraft position vector. As shown in Figure 2, the first panel is spacecraft potential also measured by EDP during an outbound orbit on September 2, 2015. The second panel is $\mathbf{E}_{\text{obs}}$ in GSE coordinates, and other electric fields are also in the same coordinates. The third panel is $-\mathbf{V}_{\text{sc}}\times\mathbf{B}$, the electric field introduced by the motion of the spacecraft in Earth frame. The fourth panel is co-rotation electric field. The fifth panel is $\boldsymbol{E}_y$ in the co-rotation frame. Subsequently, the data are smoothed with

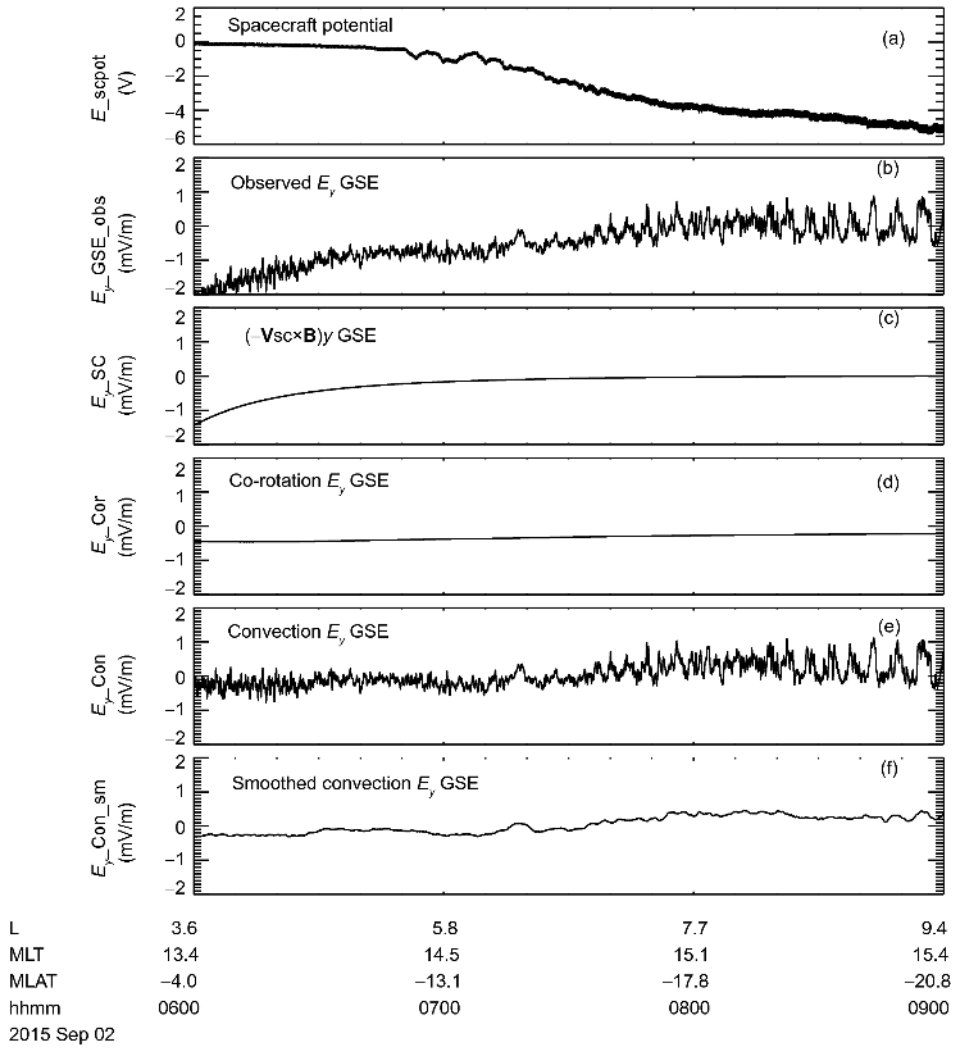

Figure 2 Example of the calculation of convection electric field in GSE coordinate from 06:00 to 09:00UT on September 2, 2015. (a) Spacecraft potential; (b) y component of $\mathbf{E}_{obs}$ in spacecraft frame; (c) y component of $\mathbf{V}_{sc}\times\mathbf{B}$; (d) y component of co-rotation electric field; (e) E_y in the co-rotation frame; (f) smoothed E_y in the co-rotation frame.

5-minute windows to filter low-frequency waves. The last panel shows the smoothed convection electric field.

We constrain our analysis in the region between L=5 to L=8 to minimize the effect of small-scale electric field structures, such as sub-auroral polarization stream (SAPS) at low L shells [32] or dipolarization front at high L shells [33,34]. SAPSs are strong sunward flows observed during active times near the plasmasheet inner edge. SAPS causes duskside flow enhancement, resulting in the radial motion of plasmapause [35,36]. SAPS can enhance the electric field at low L shells (L~2–5) during magnetic active time at duskside particularly, resulting in complicated electric field pattern around the plasmapause [21,37]. However, this kind of disturbance is beyond the scope of this study. The data inside the plasmasphere and outside the magnetopause are manually removed from the database based on spacecraft potential and plasma measurement, respectively. Visual inspection is further performed in order to remove abnormal measurements.

As we can see in Figure 2, the DC convection electric field generally has small variations in the region of interest. For each inbound or outbound orbit crossing, the DC electric field is averaged in the studied region and is considered as one data sample, hereafter referred to as E_{con}. Those data samples are removed from the database if (1) the spatial coverage of the data sample is less than 0.5 Re, or (2) the standard deviation for the data sample is more than 1 mV/m, which are usually related to data quality issues. Solar wind parameters and geomagnetic activity indices are averaged in the time period of each sample.

In total, 482 data samples of large-scale electric field are obtained based on the measurements from September 1, 2015 to October 31, 2016. These data samples cover all the magnetic local times (MLT), as shown in Figure 3. There are

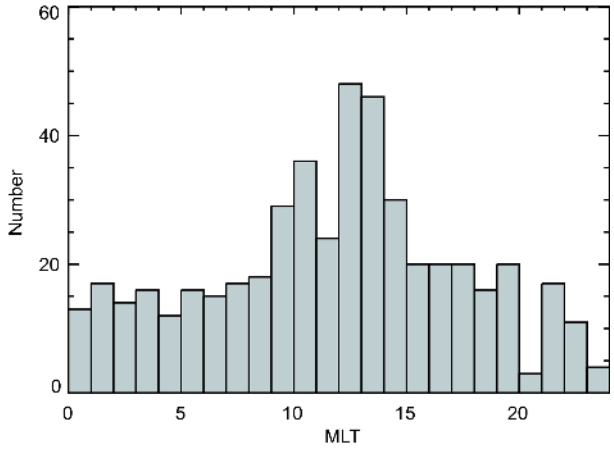

Figure 3 Distribution of the data samples over magnetic local time from September 1, 2015 to October 31, 2016.

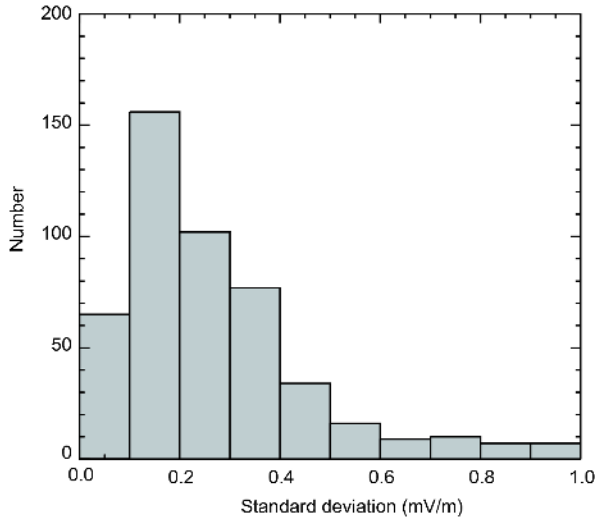

Figure 4 Distribution of the standard deviation of E_{con} for the 482 data samples.

more data samples around the noon sector than other sectors, because of the change of instrument operation after April 2016.

4 Observations

Based on the electric field database described in the previous section, we can study the characteristics of the large-scale dawn-dusk electric field. It is found that the value of the electric field observed by MMS varied between −0.4 and 0.8 mV/m, which is similar with previous results, like Baumjohann et al. [25,26] based on GEOS 2 measurements and Califf et al. [8] based on THEMIS measurements. It is also found that the averaged E_y component is positive (duskward) for 58% of the data samples. The standard deviation for each data sample is used to evaluate the variation of the electric field in the region between L=5 to L=8. As a reference, in the event with small electric field variations shown in Figure 2, the standard deviation is 0.05 mV/m. The distribution of the standard deviation for all the events is shown in Figure 4. As one can see, the largest occurrence of the standard deviation is between 0.1 and 0.2 mV/m. For about 90% of the data samples, the standard deviation is below 0.5. It therefore indicates that the electric field generally has small variations in the region between L=5 to L=8.

The dependences of the y component of the convection electric field on geomagnetic activities are further investigated based on the database, as shown in Figure 5. The correlation coefficient (CC) between E_{con} and AE, Kp and SYM_H indices are plotted in Figure 5(a)–(c) respectively. In each panel, the E_{con} is bin-averaged with the given parameter and the error bars represent the standard deviation of the mean in each bin. Those bins having <5 data samples are not included in the analysis. Overall, there are good correlations between E_{con} and geomagnetic indices, with the correlation coefficient greater than 0.9 for AE and Kp, and 0.65 for SYM_H.

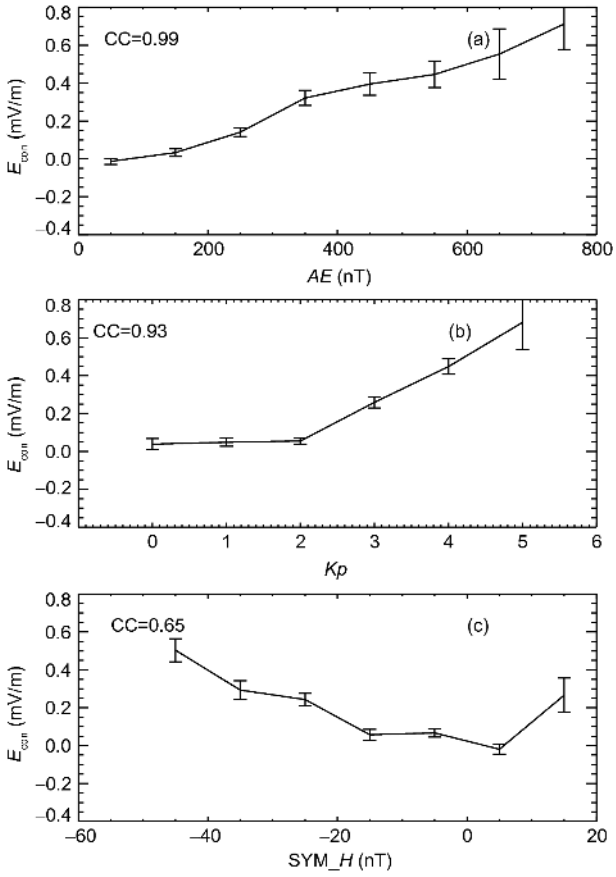

Figure 5 Correlation between E_{con} and geomagnetic indices. (a) AE; (b) Kp; (c) SYM_H.

The dependence of E_{con} with AE index is shown in Figure 5(a). The AE index indicates the intensity of geomagnetic substorms . In the case of very low AE~50 nT, E_{con}

is around 0 mV/m. While *AE* index increases, E_{con} increases nearly linearly to around 0.71 mV/m for *AE*=750 nT. Due to the limited number of data samples, the correlation study is limited for *AE*<800 nT. The correlation coefficient between E_{con} and *AE* index is as high as 0.99, suggesting a very strong correlation between them and the possibility of predicting E_{con} with *AE* index. The *Kp* index is considered to describe the strength of large-scale convection in the magnetosphere. The relationship between *Kp* index and large-scale electric field has been investigated in several previous studies [8,24]. As shown in Figure 5(b), the correlation coefficient between E_{con} and *Kp* index is around 0.93. However, different from the E_{con} variation with *AE* index, for *Kp* values below 2, E_{con} is around 0 mV/m and increases slowly with *Kp*. While *Kp* is 3 and above, E_{con} increases obviously and linearly to ~0.7 mV/m for *Kp*=5. Again, because of the limitation of data sample, the cases with *Kp*>5 is not considered in this paper.

For the SYM-H index as shown in Figure 5(c), E_{con} has a negative correlation for SYM_*H*<0, suggesting that the convection electric field enhances during geomagnetic active time. Interestingly, E_{con} also enhances for SYM_*H*>0, which is possibility related to the compression of Earth's magnetic field by the interplanetary shocks.

The dependences of the convection electric field on solar wind condition are shown in Figure 6, for solar wind speed (SW_*V*), solar wind electric field (SW_*E*), solar wind dynamic pressure (SW_*Dp*), *x* component of IMF (IMF_B_x), *y* component of IMF (IMF_B_y), and *z* component of IMF (IMF_B_z) in Figure 6(a)–(f) respectively in the same format as Figure 5.

As we can see in Figure 6, the correlation coefficient between convection electric field and SW_*E*, IMF_B_z are greater than 0.9 suggesting strong correlation between them. SW_*V* and IMF_B_x have relatively lower correlation coefficient with electric field around 0.5. The correlation coefficients between convection electric field and SW_*Dp* and IMF_B_y are less than 0.3. These results suggest that the orientation of IMF in equatorial plane and SW_*Dp* plays only minor roles in changing the convection electric field in the inner magnetosphere.

In Figure 6(f), it is shown that IMF_B_z has a negative correlation with E_{con}. For northward IMF_B_z, E_{con} value is close to 0 or negative, suggesting that there is weak convection in the magnetosphere during northward IMF period. While for southward IMF_B_z, E_{con} becomes larger as IMF_B_z turns more southward suggesting enhanced magnetosphere convection because of the enhanced coupling between solar wind and magnetosphere. The dayside reconnection due to the southward IMF may increase energy input into the magnetosphere as described by the scenario of the Dungey cycle.

5 Summary

In this paper, we use recent MMS measurements to study the large-scale convection electric field in the inner magnetosphere. It is found that the value of the convection electric field varies between −0.4 and 0.8 mV/m with small variations in the region between *L*=5 to *L*=8 outside the plasmasphere. The small-scale variations of electric field around the

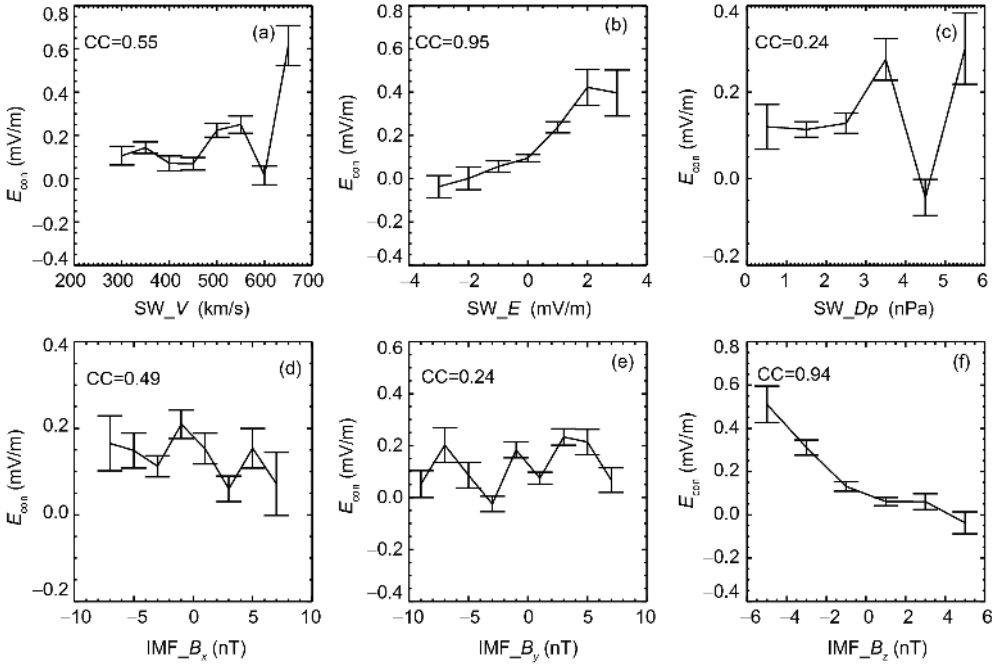

Figure 6 Correlation between E_{con} and solar wind parameters. (a) SW_*V*; (b) SW_*E*; (c) SW_*Dp*; (d) IMF_B_x; (e) IMF_B_y; (f) IMF_B_z.

plasmapause are not considered in this study, which could possibly explain the difference between this study and previous observations in terms of the radial profile of the convection electric field.

Strong correlations have been found between convection electric field and various geomagnetic indices and solar wind parameters, such as *AE*, *Kp*, SW_*E* and IMF_B_z, while for some other parameters like SW_*Dp* and IMF_B_y, the correlation is weak. The relationships found in this study generally agree with previous studies, except that we investigate more parameters here. These results provide valuable information for understanding the role of electric field in determining the inner magnetospheric dynamics.

This work was supported by the National Natural Science Foundation of China (Grant Nos. 41574154 and 41431071). We thank the FIELDS instrument team of MMS mission for making data available. We thank Dr. Yuri Khotyaintsev for helpful discussion. The solar parameters and geomagnetic indices are obtained from the OMNI database (http://omniweb.gsfc.nasa.gov).

1 Fu H S, Tu J, Song P, et al. The nightside-to-dayside evolution of the inner magnetosphere: Imager for Magnetopause-to-Aurora Global Exploration Radio Plasma Imager observations. J Geophys Res, 2010, 115: A04213
2 Thaller S A, Wygant J R, Dai L, et al. Van Allen Probes investigation of the large-scale duskward electric field and its role in ring current formation and plasmasphere erosion in the 1 June 2013 storm. J Geophys Res Space Phys, 2015, 120: 4531–4543
3 Liu X, Liu W, Cao J B, et al. Dynamic plasmapause model based on THEMIS measurements. J Geophys Res Space Phys, 2015, 120: 543–556
4 Liu X, Liu W L. A new plasmapause location model based on THEMIS observations. Sci China Earth Sci, 2014, 57: 2552–2557
5 Liu W, Tu W, Li X, et al. On the calculation of electric diffusion coefficient of radiation belt electrons with *in situ* electric field measurements by THEMIS. Geophys Res Lett, 2016, 43: 1023–1030
6 Cao J B, Ding W Z, Reme H, et al. The statistical studies of the inner boundary of plasma sheet. Ann Geophys, 2011, 29: 289–298
7 Fu H S, Cao J B, Yang B, et al. Electron loss and acceleration during storm time: The contribution of wave-particle interaction, radial diffusion, and transport processes. J Geophys Res, 2011, 116: A10210
8 Califf S, Li X, Blum L, et al. THEMIS measurements of quasi-static electric fields in the inner magnetosphere. J Geophys Res Space Phys, 2014, 119: 9939–9951
9 Weimer D R. Models of high-latitude electric potentials derived with a least error fit of spherical harmonic coefficients. J Geophys Res, 1995, 100: 19595–19607
10 Cao J B, Zhang D, Reme H, et al. Preliminary empirical model of inner boundary of ion plasma sheet. Adv Space Res, 2015, 56: 1194–1199
11 Wei Y, Pu Z, Hong M, et al. Westward ionospheric electric field perturbations on the dayside associated with substorm processes. J Geophys Res, 2009, 114: A12209
12 Wei Y, Pu Z, Hong M, et al. Long-lasting goodshielding at the equatorial ionosphere. J Geophys Res, 2010, 115: A12256
13 Wei Y, Wan W, Pu Z, et al. The transition to overshielding after sharp and gradual interplanetary magnetic field northward turning. J Geophys Res, 2011, 116: A01211
14 Kistler L M, Ipavich F M, Hamilton D C, et al. Energy spectra of the major ion species in the ring current during geomagnetic storms. J Geophys Res, 1989, 94: 3579–3599
15 Jordanova V K, Boonsiriseth A, Thorne R M, et al. Ring current asymmetry from global simulations using a high-resolution electric field model. J Geophys Res, 2003, 108: 1443
16 Ma Y D, Cao J B, Zhou G, et al. Multipoint analysis of the rapid convection event. Chin J Geophys, 2007, 1148: 189–199
17 Ding W Z, Cao J B, Zeng L, et al. Simulation studies of plasma sheet ion boundary. Chin J Geophys, 2010, 53: 1505–1514
18 Zhang D, Cao J B, Wei X H, et al. New technique to calculate electron Alfvén layer and its application in interpreting geosynchronous access of PS energetic electrons. J Geophys Res Space Phys, 2015, 120: 1675–1683
19 Liu W L, Li X, Sarris T, et al. Observation and modeling of the injection observed by THEMIS and LANL satellites during the 23 March 2007 substorm event. J Geophys Res, 2009, 114: A00C18
20 Wolf R A. Ionosphere-magnetosphere coupling. Space Sci Rev, 1975, 17: 537–562
21 Yu Y, Jordanova V K, Ridley A J, et al. Effects of electric field methods on modeling the midlatitude ionospheric electrodynamics and inner magnetosphere dynamics. J Geophys Res Space Phys, 2017, 122: 5321–5338
22 Volland H. A semiempirical model of large-scale magnetospheric electric fields. J Geophys Res, 1973, 78: 171–180
23 Stern D P. Large-scale electric fields in the Earth's magnetosphere. Rev Geophys, 1977, 15: 156–194
24 Rowland D E, Wygant J R. Dependence of the large-scale, inner magnetospheric electric field on geomagnetic activity. J Geophys Res, 1998, 103: 14959–14964
25 Baumjohann W, Haerendel G. Magnetospheric convection observed between 0600 and 2100 LT: Solar wind and IMF dependence. J Geophys Res, 1985, 90: 6370–6378
26 Baumjohann W, Haerendel G, Melzner F. Magnetospheric convection observed between 0600 and 2100 LT: Variations with *Kp*. J Geophys Res, 1985, 90: 393–398
27 Burch J L, Moore T E, Torbert R B, et al. Magnetospheric multiscale overview and science objectives. Space Sci Rev, 2016, 199: 5–21
28 Shue J H, Song P, Russell C T, et al. Magnetopause location under extreme solar wind conditions. J Geophys Res, 1998, 103: 17691–17700
29 Torbert R B, Russell C T, Magnes W, et al. The FIELDS instrument suite on MMS: Scientific objectives, measurements, and data products. Space Sci Rev, 2016, 199: 105–135
30 Ergun R E, Tucker S, Westfall J, et al. The axial double probe and fields signal processing for the MMS mission. Space Sci Rev, 2016, 199: 167–188
31 Lindqvist P A, Olsson G, Torbert R B, et al. The spin-plane double probe electric field instrument for MMS. Space Sci Rev, 2016, 199: 137–165
32 Fu H S, Tu J, Cao J B, et al. IMAGE and DMSP observations of a density trough inside the plasmasphere. J Geophys Res, 2010, 115: A07227
33 Fu H S, Khotyaintsev Y V, Vaivads A, et al. Electric structure of dipolarization front at sub-proton scale. Geophys Res Lett, 2012, 39: L06105
34 Lv L Q, Pu Z Y, Xie L. Multiple magnetic topologies in flux transfer events: THEMIS measurements. Sci China Tech Sci, 2016, 59: 1283–1293
35 Goldstein J, Sandel B R, Hairston M R, et al. Control of plasmaspheric dynamics by both convection and sub-auroral polarization stream. Geophys Res Lett, 2003, 30: 2243
36 Li C F, Zou H, Zong Q G, et al. An analysis of the correlation between the fluxes of high-energy electrons and low-middle-energy electrons in the magnetosphere. Sci China Tech Sci, 2016, 59: 1130–1136
37 Yu Y, Jordanova V, Zou S, et al. Modeling subauroral polarization streams during the 17 March 2013 storm. J Geophys Res Space Phys, 2015, 120: 1738–1750